American Mineralogist, Volume 83, pages 75–84, 1998

Single-crystal Raman spectroscopic study of dickite

CLIFF T. JOHNSTON,[1]* JOZEF HELSEN,[2] ROBERT A. SCHOONHEYDT,[3] DAVID L. BISH,[4] AND STEPHEN F. AGNEW[5]

[1] Crop, Soil and Environmental Sciences, 1150 Lilly Hall, Purdue University, West Lafayette, Indiana 47907, U.S.A.
[2] Department of Metallurgy and Materials Engineering, Materials Research Center, K.U. Leuven, De Croylaan, 2, 3001 Heverlee, Belgium
[3] Center for Surface Chemistry and Catalysis, Materials Research Center, K.U. Leuven, K. Mercierlaan, 92, 3001 Heverlee, Belgium
[4] Geology and Geochemistry, MS D469, Los Alamos National Laboratory, Los Alamos, New Mexico 87545, U.S.A.
[5] Bioscience and Biotechnology, MS J586, Los Alamos National Laboratory, Los Alamos, New Mexico 87545, U.S.A.

ABSTRACT

Raman spectra were obtained from the (001), (010), and (100) faces of a St. Claire dickite specimen of known orientation. Raman spectra collected from the (010) and (100) faces of dickite are reported for the first time and reveal vibrational features significantly different from the (001) spectra. Variations in intensities of the ν(OH) bands in polarized spectra were used to confirm previous band assignments, to determine the shape and orientation of the local Raman tensors for the OH1 and OH3 groups. The most striking polarization effect observed in the ν(OH) region of dickite was the behavior of the $a(c'c')\bar{a}$ spectrum relative to Raman and IR spectra of other orientations. Unlike previously reported spectra, the dominant feature in this spectrum was the 3643 cm^{-1} band. This large increase in intensity of the 3643 cm^{-1} band in comparison with the other ν(OH) bands was related to the fact that Raman spectra were recorded from the edge faces of dickite with the electric vector of the incident laser polarized along the c axis. This permitted observation of vibrational modes polarized along the c axis. Raman frequencies of the ν(OH) bands assigned to the OH2 and OH4 groups differ from their IR counterparts by 12 cm^{-1}, suggesting that these groups may be related by a center of symmetry. For comparison, Raman spectra in the ν(OH) region were also obtained from individual micro-crystals of kaolinite that were approximately 5 μm across the (001) face.

INTRODUCTION

Since the first structures of kaolinite and dickite were reported over sixty years ago (Pauling 1930; Gruner 1932) the structure and bonding of kaolin group minerals have continued to attract attention. However, structural details concerning the H atom are incomplete. Knowledge of the OH groups for this group of minerals is crucial to understand the many important bulk crystalline properties including interlayer bonding, stability of polytypes, structural disorder, and dehydroxylation reactions (Brindley et al. 1986; Giese 1990). OH groups also influence surface properties and reactions (Costanzo et al. 1984; Lipsicas et al. 1985; Sugahara et al. 1989; Costanzo and Giese 1990; Johnston and Stone 1990). Finally, knowledge of the positions and spectral properties of the H atoms is critical for application of quantum chemical methods to the study of phyllosilicates (Bleam 1993), particularly kaolin group minerals (Hess and Saunders 1992; Kubicki et al. 1996). Thus, the combined application of advanced spectroscopic and structural methods to the study of phyllosilicates provides essential data for developing an improved theoretical understanding of clay minerals.

Recently, Bish and Johnston (1993) determined the positions of the H atoms in dickite in a combined neutron powder diffraction, Rietveld refinement, and low-temperature Fourier transform infrared spectroscopy (FTIR) spectroscopy study of dickite. The space group of dickite is Cc. The unit-cell formula of dickite is $Al_2Si_2O_5(OH)_4$ with $Z = 4$ for a total of 16 OH groups within the unit cell. The unit cell contains four crystallographically unique OH groups each having a local site symmetry of 1 (Fig. 1). Because of the low symmetry of dickite, all four of the OH groups are expected to produce distinct ν(OH) stretching bands and all are expected to be Raman and IR active. The structural environments of the OH2 and OH4 groups are very similar, and these two OH groups were assigned (Fig. 1) to the 3655 cm^{-1} band (Bish and Johnston 1993).

In principle, vibrational spectroscopy and diffraction methods provide complementary information about the structural OH groups of clay minerals. The intrinsically small X-ray scattering cross section of the H atom limits the ability of powder X-ray diffraction methods to determine the positions of H atoms in fine-grained mineral samples (Post and Bish 1989; Moore and Reynolds 1989;

0003–004X/98/0102–0075$05.00

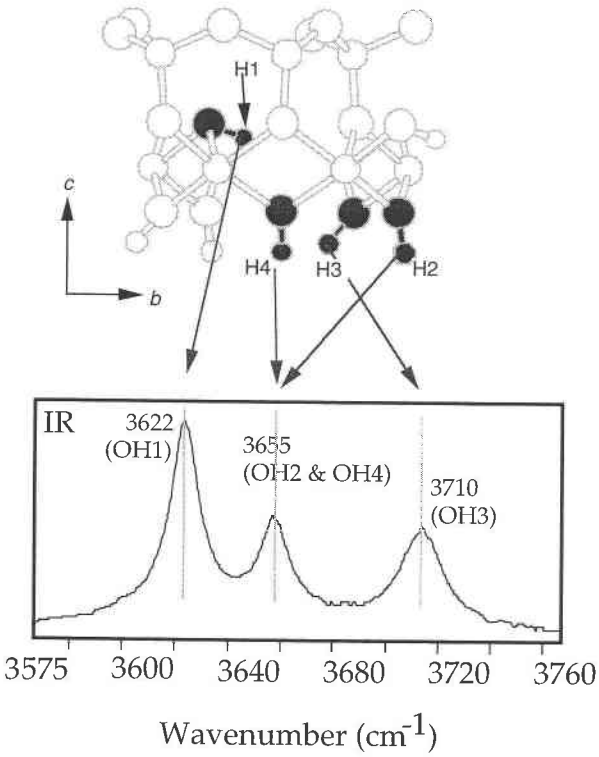

FIGURE 1. Crystal structure of dickite projected along [100] showing the positions of the four unique OH groups OH1, OH2, OH3, and OH4. In addition, the FTIR spectrum of St. Claire dickite (Bish and Johnston 1993) is shown illustrating the band assignments.

Bish 1993). In contrast, H has a very large scattering cross section for neutrons, and neutron diffraction is therefore useful for determining H locations in minerals. Likewise, the vibrational modes associated with the stretching and deformation motions of the structural OH groups of clay minerals are generally strong and sensitive to subtle changes in the local environment of the H atoms (Farmer 1974).

Attempts to determine the orientations of the structural OH groups of kaolin group minerals using IR absorption spectroscopy have met with limited success. Pleochroic studies of oriented deposits of kaolinite and dickite (Wada 1967; Rouxhet et al. 1977; Prost et al. 1987) provided qualitative information about the relative orientation of the structural OH groups tilted with respect to the (001) plane. More recently, Johnston et al. (1990) used FTIR microscopy to study single crystals of dickite and kaolinite to determine the angle of the OH groups with respect to the crystallographic *a* and *b* axes. Using a linearly polarized IR beam normal to the (001) face of single crystals of dickite, the change in IR absorbance was monitored as the electric vector of the IR beam was rotated about the *c* axis. The inferred orientations of the OH in kaolin group minerals compared poorly with the structural data (Bish and Johnston 1993).

Raman spectra collected from oriented single crystals provide a unique opportunity to correlate the observed vibrational spectra with structural information about the orientation and local environment of the OH groups. Unlike IR absorption where light must be transmitted through the sample, Raman spectroscopy is based on inelastic light scattering by the sample. This avoids a significant problem encountered in IR spectroscopy in that mineral specimens are often too thick and the IR signal is strongly attenuated by the sample. In the case of the St. Claire dickite specimen, the micrometer-sized crystals were thin enough along [001] to permit collection of IR spectra (Johnston et al. 1990). However the crystals were much too thick (on the order of 30 μm) along [010] or [100] for transmission micro-FTIR spectra to be obtained. Optical transmission of the incident laser beam through the sample is not required for Raman spectroscopy, so this restriction does not apply.

The intensity of Raman-scattered radiation from crystals depends strongly on the orientation of the crystal and the polarization of incident and scattered light. Raman scattering from an anisotropic crystal is associated with an induced change in polarizability in which amplitude depends on the orientation of the crystal, scattering geometry, and polarization of the incident and scattered radiation (Turrell 1972; Bremard et al. 1989). This study presents a complete set of polarized Raman spectra from the (001), (010), and (100) faces of a St. Claire dickite specimen of known orientation, relates the observed variation in Raman intensities of the ν(OH) bands and lattice modes to the structure of dickite, and examines the complementary relationship between IR and Raman results.

MATERIALS AND METHODS

The <325-mesh fraction (<44 μm) of a sample of dickite from St. Claire, Pennsylvania, obtained from Wards Natural Science Establishment, Inc., was used in this study. Other than sieving, the dickite sample was not treated or ground in any way. Raman spectra were obtained on a ISA-JY HR64000 micro-Raman spectrograph. An Ar^+-ion laser operating at the 514.5 nm wavelength at 100 mW of incident power was used as the excitation source. The laser power at the sample was estimated to be 10–15 mW and the laser spot size was focused to about 2 μm. Because the FWHM of the narrowest band in the ν(OH) region is greater than 4 cm^{-1}, the spectrograph slits were set to provide a spectral resolution of 3 cm^{-1}. The spectrograph used a 1800 groove/mm holographic grating and an intensified diode array detector. At 514.5 nm excitation in the ν(OH) region, approximately a 300 cm^{-1} portion of the Raman spectrum was incident upon the diode array detector.

A schematic of the Raman instrument (Fig. 2) illustrates the laboratory coordinate system used here. The excitation laser beam is incident along the *z* axis. Scattered light from the sample was collected in a 180° backscattering geometry and passed through a polarization analyzer that could be switched between two positions to pass the Raman-scattered radiation with a polarization

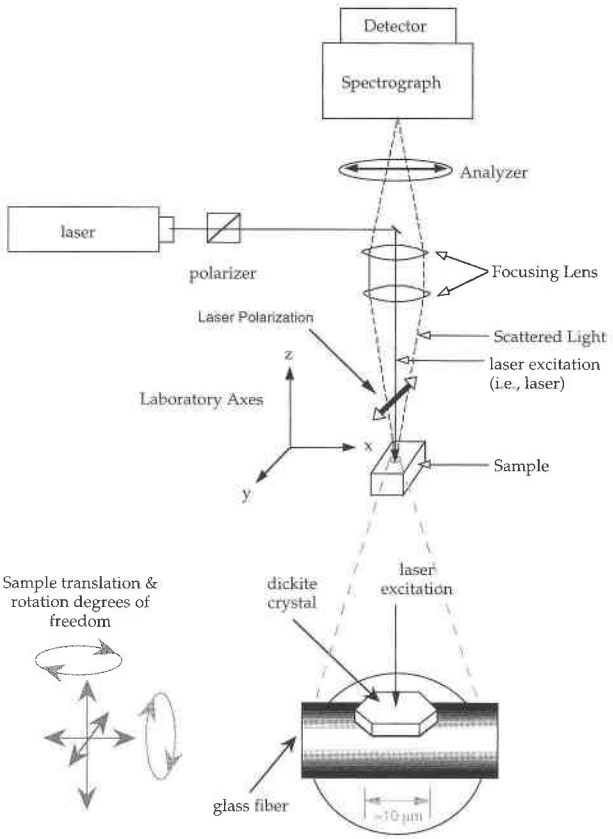

FIGURE 2. Schematic diagram of the Raman spectrograph showing the laser, polarizer, optics, sample orientation, analyzer, spectrograph, as well as the laboratory axes. An expanded view of the sample stage shows the dickite crystal attracted to the glass fiber by electrostatic attraction. The sample stage had *xyz* translation and rotation about *x* and *z*.

parallel to the *x* or *y* axis (Fig. 2). Single-crystal specimens of the St. Claire dickite were mounted on a thin glass fiber drawn from a glass tube and mounted on the translation stage of the microscope (Fig. 2). The clay crystals were electrostatically attracted to the glass fiber and could be manipulated on the glass fiber without falling off. The glass fiber mounted on the sample stage had *xyz* translation and rotation about *x* and *z*. The Raman spectrograph was coupled to an Olympus BH2 microscope, and a 50× objective was used to observe the Raman signal in this study. Initially the dickite crystal was placed with the (001) face parallel to the *x*-*y* plane of the microscope stage. Using crossed polarizers and a 550 nm quartz retardation plate, the crystallographic *a* axis was aligned parallel to the *x* axis. The laser was incident on the (001) face, the electric vector of laser was parallel to the *x* axis, and the analyzer was set parallel to the *x* axis (Fig. 2). In this configuration, the Raman scattering geometry for this spectrum is described by $c'(aa)\bar{c}'$ using the Porto notation (Swanson 1973). In this study, Raman spectra were collected at a 90° angle from the (001) face. The designation of c' is used to indicate that spectra were collected at 90° from the (001) face rather than along the *c* axis that makes an angle of 96.5° with respect to the (001) face. Because the efficiency of the spectrograph depended strongly on the polarization of the laser, spectra were obtained by positioning a selected crystal in the desired orientation while keeping the polarization of the laser constant. This approach also eliminates the need to correct for unwanted depolarization effects introduced by the beamsplitter and use of wide-aperture objectives (Bremard 1985). Optical determination of the crystallographic *a* and *b* axes for the Keokuk kaolinite sample was precluded because of the small particle size.

In the OH-stretching region, 60 accumulations were signal averaged with a count time of 5 s for each accumulation for a total observation time of 300 s. The dickite crystals produced very stable Raman spectra, and there was no evidence for visible laser damage of the dickite crystals after several hours of continuous excitation of a single specimen. In addition, very little fluorescence was observed. The low frequency region, 215 to 1200 cm^{-1}, was obtained in four separate measurements. For each sub-section, 15 accumulations were co-added with a data collection time of 5 s per scan for a total sample observation time of 60 s per sub-section. The Grams-386 program (Galactic Software) was used for spectral data manipulation and curve-fitting. In the ν(OH) region, the bands were fitted using a pseudo Voight lineshape (mixed Gaussian and Lorentzian) with a linear baseline correction and were optimized by a non-linear least-squares fitting algorithm consisting of four adjustable parameters per band (position, FWHM, intensity, and percent Lorentzian character).

RESULTS

The ν(OH) region

Polarized Raman spectra of the St. Claire Dickite specimen in the ν(OH) stretching region are shown in Figure 3, along with IR results. The Raman spectra are characterized by four bands in the ν(OH) stretching region at 3623, 3643, 3655, and 3708 cm^{-1} as shown in Figure 3. The relative intensities of these four ν(OH) bands depend strongly on the orientation of the crystal and scattering geometry. The scaling for each spectrum plotted in Figure 3 was relative to the strongest feature in that spectrum. Peak parameters of each ν(OH) band is listed in Table 1.

The $c'(aa)\bar{c}'$ spectrum (Fig. 3) corresponds to the Raman spectrum obtained from an oriented single crystal of dickite with the laser beam directed normal to the (001) face with the electric vector of the laser aligned parallel to the *a* axis. The scattered light was collected in a 180° backscattering geometry as shown in Figure 2 with the analyzer set parallel to the *a* axis. In this configuration, the bands resulting from the *aa* polarization element of the Raman polarizability tensor have maximum intensity. The *aa* spectrum is comprised of a strong feature at 3623 cm^{-1} corresponding to the OH1 group (Fig. 1) with three weaker bands appearing at 3643, 3655, and 3708 cm^{-1}

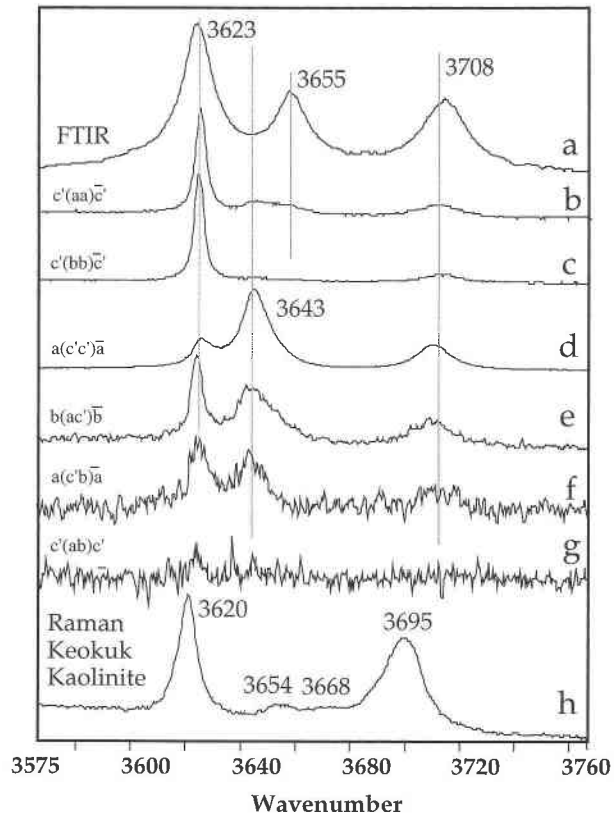

Figure 3. Polarized, single-crystal Raman spectra and FTIR absorbance spectrum (polycrystalline) of the St. Claire dickite specimen in the ν(OH) region. From top to bottom, the spectra correspond to the FTIR absorbance spectrum of the St. Claire dickite specimen, polarized single crystal Raman spectra of an oriented dickite specimen corresponding to the *c'(aa)c̄', c'(bb)c̄', a(c'c')ā, b(ac')b̄, a(c'b)ā, c'(ab)c̄'* Raman scattering geometries, and a single-crystal Raman spectrum of kaolinite from Keokuk. Raman excitation was normal to the (001) face, however, the orientation of the cyrstallographic *a* and *b* axes for this sample was not known.

corresponding to the inner surface OH groups OH2, OH3, and OH4. A detailed discussion of the FTIR spectra of dickite in the ν(OH) region has been reported by Bish and Johnston (1993).

The Raman intensities of the ν(OH) bands observed in the off-diagonal elements *c'(ab)c̄', a(bc')ā,* and *b(ac')b̄* were very weak relative to the intensities in the *c'(aa)c̄', c'(bb)c̄', and a(c'c')ā* spectra (Table 1). In obtaining the off-diagonal elements the analyzer settings were changed. Because of this change in configuration, these elements were not used for Raman tensor analysis. For example, the most intense band in the *a(bc')ā* spectrum (Fig. 3f) had an integrated area of 194 photon counts per second (Table 1) and no bands were detected in the *c'(ab)c̄* spectrum (Fig. 3g). In contrast, the integrated area of the 3643 cm^{-1} band was 67 549 photon counts per second in the *a(c'c')ā* spectrum (Fig. 3d).

Qualitatively, the Raman spectra of the ν(OH) region contain of three strong bands at 3623, 3643, and 3708 cm^{-1}. The intensity of the 3623 cm^{-1} band has maximum intensity in spectrum *bb* (Fig. 3c; Table 1). In contrast, the relative intensity of the 3623 cm^{-1} band is at a minimum in the *a(c'c')ā* spectrum (Fig. 3d) in comparison with the intensities of the 3643 and 3708 cm^{-1} bands. Comparison of the *c'(aa)c̄'* to *c'(bb)c̄'* spectra shows an increase in the intensities of 3623, 3643, and 3708 cm^{-1} bands in the *c'(bb)c̄'* spectrum. The weak band at 3655 cm-1 has maximum intensity in the *c'(aa)c̄'* spectrum (Fig. 3; Table 1). For comparison, the FTIR absorbance spectrum of dickite at 300 K is characterized by three bands at 3623, 3655, and 3708 cm^{-1} as (Fig. 3a). The observed band positions from the polarized Raman spectra are listed along with literature values for Raman spectra of kaolinite, dickite, and nacrite in Table 2.

Single-crystal Raman spectra of a Keokuk kaolinite specimen in the ν(OH) region (Fig. 3 bottom) are characterized by two strong bands at 3620 and 3695 cm^{-1} and two weak bands at 3652 and 3668 cm^{-1}. The crystals of Keokuk kaolinite were much smaller (and considerably thinner) than those of the St. Claire dickite; they mea-

Table 1. Band positions, intensities, linewidths and Lorentzian character of ν(OH) bands of dickite in the 5* Raman scattering geometries

	3623 cm^{-1} band				3643 cm^{-1}				3654 cm^{-1} band				3707 cm^{-1} band			
Polarization element	Band pos	Integrated area	Full width at half maximum	Fractional Lorentzian lineshape	Band pos	Integrated area	Full width at half maximum	Fractional Lorentzian lineshape	Band pos	Integrated area	Full width at half maximum	Fractional Lorentzian lineshape	Band pos	Integrated area	Full width at half maximum	Fractional Lorentzian lineshape
c'(aa)c̄'	3622.9	6862	4.6	0.9	3642.9	2162	13.0	1.0	3654.0	1073	12.2	0.5	3707.5	2595	16.5	0.7
c'(bb)c̄'	3622.8	17764	4.2	0.8	3644.5	2641	22.8	1.0	3656.2	260	9.0	0.0	3708.8	5305	17.4	0.8
a(c'c')ā	3623.9	11685	7.9	0.6	3642.8	67549	12.2	1.0	nd	nd	nd	nd	3706.3	23843	14.9	0.8
a(c'b)ā	3623.1	2054	4.9	1.0	3642.8	3568	13.1	1.0	3654.0	370	10.9	0.0	3706.7	1946	16.0	1.0
b(ac')b̄	3624	194	8.1	1.0	3642.3	186	11.3	0.7	nd	nd	nd	nd	3708.2	99	16.1	0.7
Average	3623.3		5.9	0.9	3643.1		14.5	0.9	3654.7		10.7	0.2	3707.5		16.2	0.8
Std. dev.	0.6		1.9	0.2	0.8		4.7	0.1	1.3		1.6	0.3	1.0		0.9	0.1

* Parameters for c'(ab)c̄' were not determined.

TABLE 2. Comparison of single crystal Raman frequencies with published spectra and assignments for kaolinite, dickite, and nacrite

Dickite				Kaolinite			Nacrite	
Polarized single-crystal Raman St. Claire dickite (this study)			Raman polycryst. Nowa Ruda dickite*	Raman polycryst. Keokuk kaolinite*	Raman polycryst. KGa-1 kaolinite†	Raman polycryst. API #9 kaolinite‡	Raman polycryst. Yama Gata nacrite*	
c′(aa)c̄′	c′(bb)c̄′	a(c′c′)ā						Type of vibrational motion
			120	120			120	
			132	132	130	130	132	
					141	141	140	
			178					
			198	200	201	202	197	
223	223							
248	245	246	245	248	244	244	238	
271	270	270	268	272	271	271	268	Structural lattice modes
339	339	339	336	338	335	334	332	
					397	396		
			420	420			418	
437	439	437	434	434	431	430	433	
468	484	462	463	461	461	462	462	
525	525				512	511		
750	750	749	748	749	750	752	748	
			792	791	790	790		
799	797	797					798	
847	846							
921	919		916	916	915	915	916	OH deformation (bending modes)
			935	935	940	941	935	
		1049	1050	1048				Si-O stretching modes
							1085	
			1104	1105			1102	
3623	3623	3623	3623	3620	3620	3620	3618	
3643	3643	3643	3648				3628	
3655	3655			3650	3652	3652	3634	O-H stretching modes
				3668	3668	3668	3650	
				3682	3688	3688		
			3683	3692	3695	3696	3698	
3708	3708	3708	3700					

* Wiewora et al. 1979.
† Johnston et al. 1985.
‡ IR frequencies compiled from (Farmer 1974; Ledoux and White 1964; Wada 1967; Ishii et al. 1967; Estep et al. 1968; Larson et al. 1972; and Rouxhet et al. 1977).

sured about 5 μm across the (001) face, on average. The intensity of the Raman signal was much lower for this sample and longer data acquisition times were required. The crystal was rotated about the c' axis and several spectra were obtained to observe the change in relative intensity of the ν(OH) bands. Although the orientation of the crystallographic a and b axes for this sample could not be determined using crossed polarizers because of the small thickness of the crystal, the spectra were strongly influence by rotation about the c axis.

Lattice modes

Polarized Raman spectra of the St. Claire Dickite specimen in the 200–1200 cm^{-1} region are shown in Figure 4. Similar to the ν(OH) region, the low-frequency modes vary strongly in intensity among the scattering geometries used here. Spectra were not collected below 200 cm^{-1} because of a strong Rayleigh-scattering wing and the stray-light characteristics of the spectrograph. Several strong Raman bands exist in the 100–200 cm^{-1} region that were not recorded here (Wiewiora et al. 1979; Johnston et al. 1985; Michaelian 1986). In general, good agreement exists between the observed band positions ob-

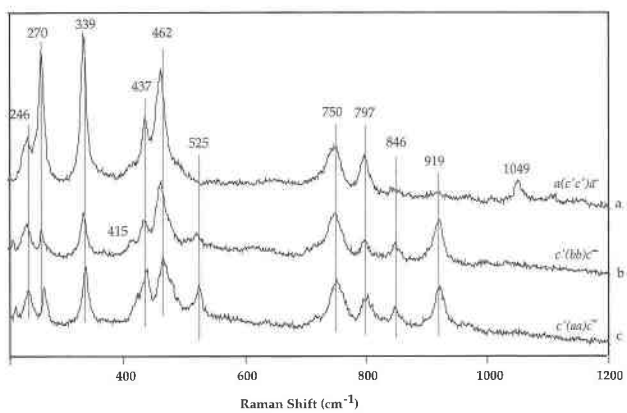

FIGURE 4. Polarized, single-crystal Raman spectra of the St. Claire dickite specimen in the 200–1200 cm^{-1} region. From top to bottom, the spectra correspond to the $c'(aa)\bar{c}'$, $c'(bb)\bar{c}'$, and $a(c'c')\bar{a}$ polarization elements.

TABLE 3. Assignment of the ν(OH) bands of dickite with a comparison of Raman-derived OH orientations with OH geometries from crystal structure

Assignments	Peak position (cm^{-1})	Intensity ratio (I_{bb}/I_{aa})	Angle of OH group with *b* axis from crystal structure*	Angle with (001) plane calculated from crystal structure*	Raman tensor analysis
OH1	3623	2.59	33.8	−1.3°	0.25
OH2	3643	1.22	41.3	75.5°	n.a.
OH3	3707	1.94	34.6	51.9°	0.47
OH4	3643	1.22	89.9	74.1°	n.a.

Notes: n.a. = not applicable because the OH stretching bands of the OH2 and OH4 groups are degenerate.
* Bish and Johnston 1993.

served in the polarized Raman spectra with published IR and Raman spectra of kaolin group minerals. All of the observed bands in Figure 4 have been reported previously with the exception of the band at 846 cm^{-1} observed in the $c'(aa)\bar{c}'$ and $c'(bb)\bar{c}'$ spectra. The band positions of the polarized Raman spectra are tabulated with published positions of Raman bands reported for kaolinite, dickite, and nacrite in Table 2. The bands at 270, 339, 462, and 1049 cm^{-1} showed maximum intensity in the $a(c'c')\bar{a}$ spectrum (Fig. 4). The 1049 cm^{-1} band was not observed in either the $c'(aa)\bar{c}'$ or $c'(bb)\bar{c}'$ spectra (Fig. 4). The OH deformation band assigned to the inner OH group (OH1), on the other hand, showed maximum intensity in the $c'(aa)\bar{c}'$ and $c'(bb)\bar{c}'$ spectra and is not observed in the $a(c'c')\bar{a}$ spectrum. The OH deformation band at 937 cm^{-1} assigned to the inner-surface OH groups OH2, OH3, and OH4 was not observed in the Raman spectrum (Table 2).

Discussion

The 3623 cm^{-1} band

This band has been unambiguously assigned to the OH1 group (Johnston et al. 1990; Bish and Johnston 1993). The OH1 group is oriented essentially within the *a-b* plane (Table 3; Figs. 1 and 5b, 5c) and consequently has the longest OH vector projected onto the (001) plane of the four structural OH groups (Fig. 5a). As a result, this band has the largest Raman intensity of all the ν(OH) bands observed in the $c'(aa)\bar{c}'$ and $c'(bb)\bar{c}'$ spectra. The shape of the local Raman tensor for this band is a long, thin polarizability ellipsoid directed along the H-O bond axis (see Appendix). The ratio of polarizability $r = \alpha_{xx}/\alpha_{zz} = \alpha_{yy}/\alpha_{zz}$ is 0.25, as calculated in the appendix where the *z* axis is defined by the H-O bond axis as shown in Appendix Figure 1. In other words, the largest change in polarizability of this mode is along the H-O bond axis. This band is IR-active (Fig. 3a) and its IR counterpart is also the most intense ν(OH) band in the IR spectrum of dickite (Prost et al. 1987; Bish and Johnston 1993). The FWHM value for this band is about 4.5 cm^{-1} (Table 1). Upon cooling to 12 K the band observed in the IR spectrum decreased in frequency to 3619 cm^{-1}. The corresponding band in kaolinite occurs at 3620 cm^{-1} and is shown in Figure 3h. On the basis of the large change in intensity of the 3623 cm^{-1} band upon rotation about the c' axis, it is suggested that the observed change in intensity could readily be used to spectroscopically determine the orientation of the crystallographic *a* and *b* axes.

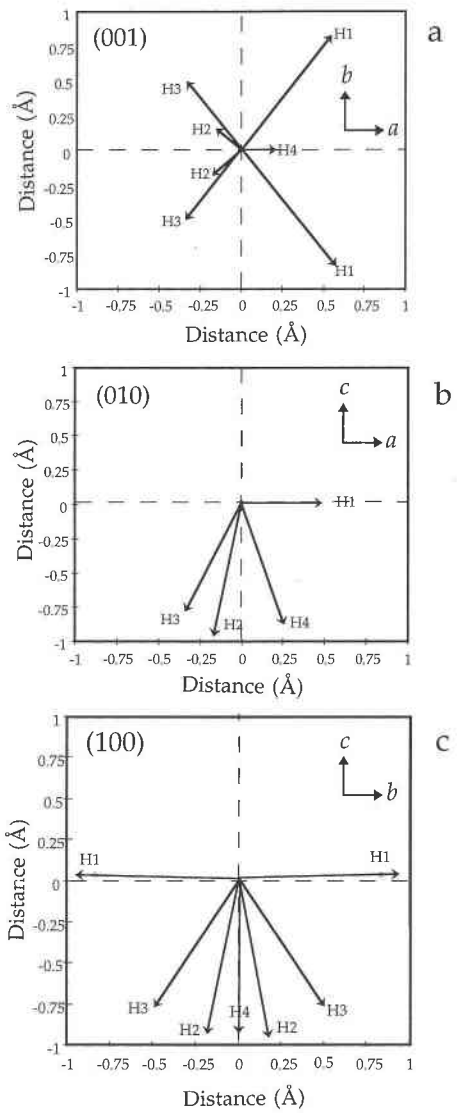

FIGURE 5. Projection of the four OH groups of dickite on the (001), (010), and (100) faces. The positions of the H atoms are indicated by the arrows with the O atom for each OH group set at a common origin.

The 3643 and 3655 cm^{-1} bands

The most striking polarization effect observed in the ν(OH) region of dickite in the $a(c'c')\bar{a}$ spectrum relative to the other Raman or IR spectra shown in Figure 3. The relative intensity pattern for the $a(c'c')\bar{a}$ spectrum is completely different from those of the $c'(aa)\bar{c}'$, $c'(bb)\bar{c}'$, and $c'(ab)\bar{c}'$ spectra. The strong increase in intensities for the

3643 and 3708 cm^{-1} bands and concomitant decrease in intensity of the 3623 cm^{-1} is due to the fact that the inner-surface OH groups are tilted toward the c axis. In particular, the 3643 cm^{-1} band is the dominant ν(OH) band in the $a(c'c')\bar{a}$ spectrum. In fact, this band in the $a(c'c')\bar{a}$ spectrum was the most intense Raman-active ν(OH) band observed among all of the crystal orientations (Table 1). The change in relative intensities can be explained qualitatively by the OH projection vectors shown in Figure 5b. Unlike the OH1 group that is oriented nearly parallel with the (001) plane, the OH2, OH3, and OH4 groups are tilted between 52 and 76° with respect to the (001) plane (Figs. 5b and 5c). Thus, by rotation of the dickite crystal on edge with the electric vector oriented along the c' axis, the Raman-scattering cross sections of the OH2, OH3, and OH4 groups are significantly enhanced. The single-crystal Raman spectra reported here represent the first time Raman spectra have been collected from the edge of a specimen 1:1 phyllosilicate of known orientation. These data agree qualitatively with the spectra reported recently by Frost et al. (1996), who examined the spectra of the San Juanito dickite specimen. Their spectra show similar trends in the ν(OH) region, however, the crystallographic orientation of their sample was not determined.

The single-crystal Raman spectra are described by three strong ν(OH) bands at 3623, 3643, and 3708 cm^{-1} (Fig. 3). In comparison, the room temperature FTIR absorbance spectrum of the St. Claire dickite is also characterized by three strong bands at 3622, 3655, and 3710 cm^{-1} (Fig. 3a). As shown in Figure 3a, the positions of 3622 and 3710 cm^{-1} bands in the FTIR spectrum agree well with the frequencies of the Raman bands. These bands are assigned to the ν(OH) modes of the OH1 and OH3 groups, respectively. A noticeable difference in frequency is observed, however, between the position of the IR-active band at 3655 cm^{-1} and its apparent Raman counterpart at 3643 cm^{-1} (Fig. 3). The 3655 cm^{-1} band observed in the FTIR spectrum (Fig. 3a) was assigned to the OH2 and OH4 groups by Bish and Johnston (1993) on the basis of its unusual change in frequency, distinct line-narrowing behavior upon cooling, and strong pleochroic character. A similar difference in the IR and Raman frequencies was also reported by Wiewiora et al. (1979), although no explanation was given.

There are two potential explanations for the 12 cm^{-1} difference in frequency between the Raman- and IR-active bands and both are related to the difference in selection rules of IR and Raman spectroscopy. Whereas a vibrational mode is Raman active if the mode produces a change in the induced polarizability, IR activity is associated with a change in the induced dipole moment. The first explanation is that the ν(OH) bands of the OH2 and OH4 groups are coupled oscillators. The observed difference in frequency of the OH2 and OH4 groups suggest that a local center of symmetry exists and the "Rule of Mutual Exclusion" applies. This rule states that if a molecule has a center of symmetry, vibrations cannot be both IR and Raman active. In this case, the vibrational frequencies of the OH2 and OH4 groups combine to form a symmetric and an asymmetric ν(OH) component. The symmetric ν(OH) vibration is observed mainly in the Raman spectrum at 3643 cm^{-1} and the corresponding asymmetric ν(OH) band is observed predominantly in the IR spectrum at 3655 cm^{-1}. It is interesting to note that a weak band at 3655 cm^{-1} is observed in the aa spectrum shown in Figure 3b. This weak band may be attributed to a small amount of Raman activity of the asymmetric ν(OH) stretch band observed primarily in the IR spectrum (Fig. 3a).

A second explanation is due to dispersive effects resulting from the fact that the induced dipole moment is susceptible to longer range effects within the crystal than the change in polarizability. In this case, the IR-active mode is always shifted to lower frequencies compared with its Raman counterpart (Turrell 1972). In this study, however, the Raman band at 3643 cm^{-1} occurs at a lower frequency than the IR band at 3655 cm^{-1} and the former explanation is more likely.

On the basis of this Raman and IR spectra comparison, the 3643 cm^{-1} band is assigned to the symmetric ν(OH) band of a coupled oscillator involving OH2 and OH4 groups. Additional support for this assignment comes from the large oscillator strength of this vibrational mode observed in the $c'c'$ spectrum. The integrated intensity of the 3643 cm^{-1} band is 2.8 times greater than that of the 3708 cm^{-1} band (Table 1). The $a(c'c')\bar{a}$ polarization element provides a unique opportunity to examine the vibrational modes of the dickite crystal normal to the (001) face. The relative intensity of this group in comparison with the other ν(OH) bands is larger than can be assigned to a single OH group and supports the assignment of this ν(OH) band to two OH groups.

These results are in agreement with the observed dichroic behavior of the 3655 cm^{-1} band in the IR absorption spectrum (Prost et al. 1987). The dichroic character is defined as the change in IR intensity upon tilting the sample with respect to the plane of polarization of the incident IR beam. Because most of the dickite particles are oriented with the (001) faces parallel to the deposition surface, the IR cross-section of the OH2, OH3, and OH4 groups is small (Fig. 5). Upon tilting the dickite crystal with respect to the (001) plane, the IR cross-section of these OH oscillators is increased and the 3655 and 3710 cm^{-1} bands increase in intensity. The 3655 cm^{-1} band has the highest dichroic character of any of the dickite OH bands, consistent with the orientation angles of the OH2 and OH4 (Table 3; Figs. 1 and 5).

The 3708 cm^{-1} band

The highest frequency ν(OH) band in the Raman spectrum occurs at 3708 cm^{-1} and is assigned to the OH3 group. This band also occurs in the FTIR absorbance spectrum (Fig. 3a) at approximately the same position (Bish and Johnston 1993). This OH group makes an angle of 52° with the 001 plane and has the longest interlayer

O–H. . .O distance of 3.14 Å of the inner surface OH groups. Unlike the other ν(OH) bands of dickite, this band increases in frequency by over 20 cm^{-1} upon cooling to 12 K and this increase is attributed to the long interlayer O-H···O distance. The shape of the polarizability ellipsoid for this band determined from the variation in Raman intensities is $r = \alpha_{xx}/\alpha_{zz} = \alpha_{yy}/\alpha_{zz} = 0.47$, which compares with a value of 0.25 for the 3623 cm^{-1} band (see appendix for calculations). Thus, the polarizability ellispoid is more spherical with an increased contribution from α_{xx} and α_{yy} (Table 3).

Acknowledgments

The authors thank Walter Keller for providing the Keokuk kaolinite specimen and Anant Ramdas for helpful discussions about the local Raman tensor analysis. One of the authors (CTJ) would like to express his appreciation for financial support from the Katholieke Universitiet in Leuven, Belgium, during a sabbatical leave. In addition, the authors thank Dr. Alian Wang and an anonymous reviewer for their critical review comments on the manuscript.

References cited

Bish, D.L. (1993) Studies of clays and clay minerals using X-ray powder diffraction and the rietveld method. In R.C. Reynolds and J.R. Walker, Eds., Computer applications to X-ray powder diffraction analysis of clay minerals, p. 79–122. Clay Minerals Society, Boulder.

Bish, D.L. and Johnston, C.T. (1993) Rietveld refinement and fourier transform infrared spectroscopic study of the dickite structure at low temperature. Clays and Clay Minerals, 41, 297–304.

Bleam, W.F. (1993) Atomic theories of phyllosilicates: Quantum chemistry, statistical mechanics, electrostatic theory, and crystal chemistry. Reviews of Geophysics, 31, 51–73.

Bremard, C., Dhamelincourt, P., Laureyns, J., and Turrell, G. (1985) The effect of high-numerical-aperture objectives on polarization measurements in micro-Raman spectrometry. Applied Spectroscopy, 39, 1036–1039.

Bremard, C., Laureyns, J., and Turrell, G. (1989) Polarization measurements in Raman microspectroscopy: III. Optical properties and sample orientation. Journal de Chimie physique, 86, 1246–1251.

Brindley, G.W., Kao, C., Harrison, J.L., Lipsicas, M., and Raythatha, R. (1986) Relation between structural disorder and other characteristics of kaolinites and dickites. Clays and Clay Minerals, 34, 239–249.

Costanzo, P.M. and Giese, R.F. (1990) Ordered and disordered organic intercalates of 8.4-Å synthetically hydrated kaolinte. Clays and Clay Minerals, 38, 160–170.

Costanzo, P.M., Giese, R.F., and Lipsicas, M. (1984) Static and dynamic structures of water in hydrated kaolinites: I. The static structure. Clays and Clay Minerals, 32, 419–428.

Estep, P.A. and Karr, C. (1968) The infrared spectrum of dawsonite. American Mineralogist, 53, 305–309.

Farmer, V.C. (1974) The layer silicates. In V.C. Farmer, Ed., The infrared spectra of minerals, p. 331–335. Minerals Society, London.

Fripiat, J.J. and Toussaint, F. (1963) Dehydroxylation of kaolinite: II. Conductometric measurements and infrared spectroscopy. Journal of Physical Chemistry, 67, 30–36.

Frost, R.L.; Fredericks, P.M., and Shurvell, H.F. (1996) Raman microscopy of some kaolinite clay minerals. Canadian Journal of Applied Spectroscopy, 41, 10–14.

Giese, R.F. (1990) Kaolin minerals: Structures and stabilities. In Mineralogical Society of America Reviews in Mineralogy, 19, 29–66.

Gruner, J.W. (1932) The crystal structure of dickite. Zeitschrift für Kristallographie, 83, 394–404.

Hess, A.C. and Saunders, V.R. (1992) Periodic ab initio Hartree-Fock calculations of the low symmetry mineral kaolinite. Journal of Physical Chemistry, 96, 4367–4374.

Ishii, M., Shimanouchi, T., and Nakahira, M. (1967) Far-IR absorption spectra of layer silicates. Inorganic Chimica Acta, 1, 387-392.

Johnston, C.T. (1990) Fourier transform infrared and Raman spectroscopy. In D.L. Perry, Ed., Instrumental surface analysis of geologic materials, p. 121–155, VCH, New York.

Johnston, C.T. and Stone, D.A. (1990) Influence of hydrazine on the vibrational modes of kaolinite. Clays and Clay Minerals, 38, 121–128.

Johnston, C.T., Sposito, G., and Birge, R.R. (1985) Raman spectroscopic study of kaolinite in aqueous suspension. Clays and Clay Minerals, 33, 483–489.

Johnston, C.T., Agnew, S.F., and Bish, D.L. (1990) Polarized single-crystal fourier-transform infrared microscopy of ouray dickite and keokuk kaolinite. Clays and Clay Minerals, 38, 573–583.

Kubicki, J.D., Blake, G.A., and Apitz, S.E. (1996) Ab initio calculations on aluminosilicate Q^3 species: Implications for atomic structures of mineral surfaces and dissolution mechanisms of feldspars. American Mineralogist, 81, 789–799.

Ledoux, R.L. and White, J.L. (1964) Infrared study of selective deuteration of kaolinite and halloysite at room temperature. Science, 145, 47–49.

Lipsicas, M., Straley, C., Costanzo, P.M., and Giese, R.F. (1985) Static and dynamic structure of water in hydrated kaolinites. Journal of Colloid and Interface Science, 107, 221–230.

Maiti, G.C. and Freund, F. (1981) Dehydration related proton conductivity in kaolinite. Clay Minerals, 16, 395–413.

Malengreau, N., Muller, J.P., and Calas, G. (1994) Fe-speciation in kaolins: a diffuse reflectance study. Clays and Clay Minerals, 42, 137–145.

Michaelian, K.H. (1986) The Raman spectrum of kaolinite #9 at 21 °C. Canadian Journal of Chemistry, 64, 285–289.

Moore, D.M. and Reynolds, R.C. (1989) X-ray diffraction and the identification and analysis of clay minerals, p. 1–332. Oxford University Press, Oxford.

Murad, E. (1997) Identification of minor amounts of anatase in kaolins by Raman spectroscopy. American Mineralogist, 82, 203–206.

Pauling, L. (1930) The structure of chlorites. Proceedings of the National Academy of Science, 16, 578–582.

Post, J.E. and Bish, D.L. (1989) Rietveld refinement of crystal structures using powder X-ray diffraction data. In Mineralogical Society of America Reviews in Mineralogy, 20, 277–305.

Prost, R., Dameme, A., Huard, E., and Driard, J. (1987) Low temperature (300-5K) IR study of structural OH groups of kaolinite, dickite, and nacrite. In L.G. Schultz, H. van Olphen, and F.A. Mumpton, Eds., Proceedings of the International Clay Conference, Denver 1985, p. 17–23. Clay Minerals Society, Boulder.

Rouxhet, P.G., Samudacheata, N., Jacobs, H., and Anton, O. (1977) Attribution of the OH stretching bands of kaolinite. Clay Minerals, 12, 171–178.

Sacuto, A., Desmicht, R., and Jegoudez, J. (1996) Straightforward identification of the a and b crystalline axes in $YBa_2Cu_3O_7$ single crystals by a polarizing microscope set-up. Superconductivity Science and Technology, 9, 483–487.

Stubican, V. and Roy, R. (1961) A new approach to assignment of infrared adsorption bands in layer-structure silicates. Zeitschrift für Kristallographie, 115, 200–214.

Sugahara, Y., Satokawa, S., Yoshioka, K., Kuroda, K., and Kato, C. (1989) Kaolinite-pyridine intercalation. Clays and Clay Minerals, 37, 143–150.

Swanson, B.I. (1973) General notation for polarized Raman scattering from gases, liquids, and single crystals. Applied Spectroscopy, 27, 382–385.

Tsuboi, M., Ueda, T., and Ushizawa, K. (1995) Localized Raman tensors in some biopolymers. Journal of Molecular Structure, 352/353, 509–517.

Tsuboi, M., Ueda, T., Ushizawa, K., and Nagazhima, N. (1995) Raman tensor of adenine residue for the 1580 cm^{-1} vibration and its orientation in a biopolymer. Journal of Raman Spectroscopy, 26, 745–749.

Turrell, G. (1972) Infrared and Raman spectra of crystals, p. 1–384. Academic, London.

Ueda, T., Ushizawa, K., and Tsuboi, M. (1996) Local Raman tensors of cytidine and their orientations in poly(rI)-poly(rC) 1. Journal of Molecular Structure, 379, 171–187.

Wada, K. (1967) A study of hydroxyl groups in kaolin minerals utilizing selective-deuteration and infrared spectroscopy. Clay Minerals, 7, 51–61.

Wieckowski, T. and Wiewiora, A. (1976) New approach to the problem of the interlayer bonding in kaolinite. Clays and Clay Minerals, 24, 219–223.

Wiewiora, A., Wieckowski, T., and Sokolowska, A. (1979) The Raman spectra of kaolinite sub-group minerals and of pyrophyllite. Archiwum Mineralogiczne, 35, 5–14.

Wilson, E.B., Decius, J.C., and Cross, P.C. (1955) Molecular vibrations: The theory of infrared and Raman vibrational spectra, p. 1–388. Dover Publications, New York.

Manuscript received December 20, 1996
Manuscript accepted September 11, 1997

Appendix: Theory

In general, the Raman tensor of a crystal α_{XYZ} is related to the Raman tensor of a constituent molecule α_{xyz} by

$$\alpha_{XYZ} = \hat{u}\ \alpha_{xyz}\ u \tag{1}$$

The transformation matrix $\hat{u}$ is defined following Wilson et al. (1955). Here, (x,y,z) is a rectangular coordinate system fixed on the molecule in question, and it is the principal axis system of the Raman tensor of a localized vibration of the molecule. This transformation matrix maps the molecular axes for a particular vibrational mode in xyz onto the laboratory axes in XYZ.

For every crystal system, the individual components of the crystalline Raman tensor are given as a function of the components of the molecular Raman tensor by the following set of equations (Ueda et al. 1996).

$$\alpha_{XX} = l_x^2\alpha_{xx} + l_y^2\alpha_{yy} + l_z^2\alpha_{zz} \tag{2}$$

$$\alpha_{YY} = m_x^2\alpha_{xx} + m_y^2\alpha_{yy} + m_z^2\alpha_{zz} \tag{3}$$

$$\alpha_{ZZ} = n_x^2\alpha_{xx} + n_y^2\alpha_{yy} + n_z^2\alpha_{zz} \tag{4}$$

$$\alpha_{XY} = l_x m_x\alpha_{xx} + l_y m_y\alpha_{yy} + l_z m_z\alpha_{zz} \tag{5}$$

$$\alpha_{YZ} = m_x n_x\alpha_{xx} + m_y n_y\alpha_{yy} + m_z n_z\alpha_{zz} \tag{6}$$

$$\alpha_{XZ} = n_x l_x\alpha_{xx} + n_y l_y\alpha_{yy} + n_z l_z\alpha_{zz}. \tag{7}$$

The xyz coordinate system is transformed into the space-fixed crystal (i.e., abc) coordinate system by means of the direction cosines (i.e., l, m, n) relating rotating to nonrotating axes functions of Eularian angles (Wilson et al. 1995). In the case of the dickite which is monoclinic, the laboratory X and Y axes are set to be coincident with the a and b axes and c' is defined as the normal to the a-b plane and is coincident with Z. Thus, Equations 2–7 can be written as

$$\alpha_{aa} = l_x^2\alpha_{xx} + l_y^2\alpha_{yy} + l_z^2\alpha_{zz} \tag{8}$$

$$\alpha_{bb} = m_x^2\alpha_{xx} + m_y^2\alpha_{yy} + m_z^2\alpha_{zz} \tag{9}$$

$$\alpha_{c'c'} = n^2\alpha_{xx} + n_y^2\alpha_{yy} + n_z^2\alpha_{zz} \tag{10}$$

$$\alpha_{ab} = l_x m_x\alpha_{xx} + l_y m_y\alpha_{yy} + l_z m_z\alpha_{zz} \tag{11}$$

$$\alpha_{bc'} = m_x n_x\alpha_{xx} + m_y n_y\alpha_{yy} + m_z n_z\alpha_{zz} \tag{12}$$

$$\alpha_{ac'} = n_x l_x\alpha_{xx} + n_y l_y\alpha_{yy} + n_z l_z\alpha_{zz}. \tag{13}$$

In these equations, a set of molecular axes, or local axes, are defined that describe the vibrational mode of interest. In this case, The H-O bond defines the orientation of the z axis, the x axis is contained within the plane defined by the three atoms Al_1-O-H normal to z. Finally, the y axis is orthogonal to z and x. The local molecular axes for the OH1 group are shown in relation to the projections on (001) and (010) in Appendix Figure 1. The xyz coordinate system is transformed into the space fixed crystal (i.e., abc') coordinate system by means of the direction cosines relating rotating to nonrotating axes as functions of Eulerian angles (Wilson et al. 1955)

The Raman tensor of a molecule has six components $\alpha_{xx},\ldots\alpha_{zx}$, but when the principal axes x, y, and z are adopted, only three diagonal components α_{xx}, α_{yy}, and α_{zz} are not zero (Tsuboi et al. 1995a, 1995b; Ueda et al. 1996). The orientation of the principal axis system is defined by three independent parameters (nine elements of direction cosines minus six orthonormal conditions) of three Eulerian angles θ, ϕ, and χ

Appendix Table 1. Directional cosine transformation matrices

	OH1 group*			OH3 group†		
	a	b	c	a	b	c
X	−0.687	−0.474	−0.550	−0.883	0.460	0.091
y	−0.468	−0.290	0.834	−0.316	−0.728	0.607
z	−0.555	0.831	−0.022	0.345	0.508	0.788

* Eulerian angles are $\theta = 1.593$, $\phi = 2.259$, $\chi = 0.987$.
† Eulerian angles are $\theta = 0.662$, $\phi = 0.973$, $\chi = 1.719$.

$$\begin{array}{c} \\ x \\ y \\ z \end{array}\begin{array}{c} \begin{array}{ccc} \text{a} & \text{b} & \text{c}' \end{array} \\ \begin{bmatrix} \cos(\theta)\cos(\phi)\cos(\chi) - \sin(\phi)\sin(\chi) & \cos(\theta)\sin(\phi)\cos(\chi) + \cos(\phi)\sin(\chi) & -\sin(\theta)\cos(\chi) \\ -\cos(\theta)\cos(\phi)\sin(\chi) - \sin(\phi)\cos(\chi) & -\cos(\theta)\sin(\phi)\sin(\chi) + \cos(\phi)\cos(\chi) & \sin(\theta)\sin(\chi) \\ \sin(\theta)\cos(\phi) & \sin(\theta)\sin(\phi) & \cos(\theta) \end{bmatrix} \end{array}. \tag{14}$$

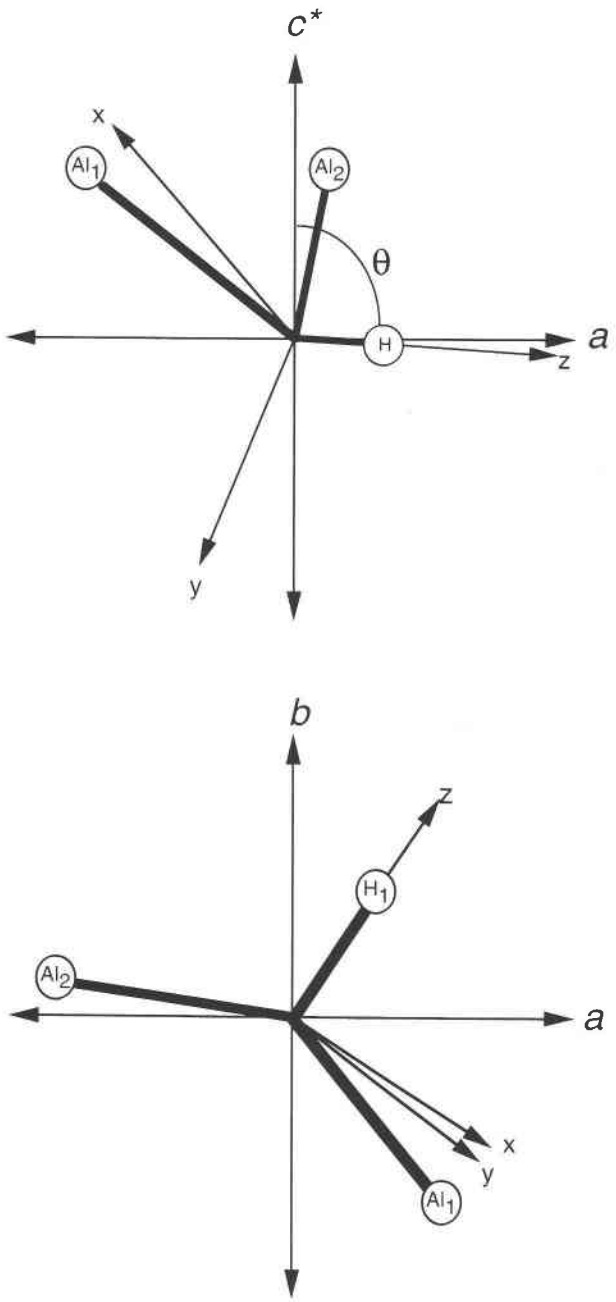

Appendix Figure 1. Principal (i.e., local) axis system (x, y, z) of the local Raman tensor for localized vibration of the OH1 group projected onto the crystal axis system (a, b, c').

The two coordinate systems are shown in Appendix Figure 1 for the inner OH group of dickite (OH_1). The angles θ, χ, and ϕ are the ordinary polar coordinates of the z axis in the abc' system as defined by Wilson et al. (1955).

The main objective here is to relate the change in intensities of the OH stretching bands obtained along the crystallographic axes (e.g., I_{aa}, I_{bb}) to the shape and orientation of the Raman tensor (i.e., α_{xx}, α_{yy}, α_{zz}) for each of the OH stretching bands. We are interested only in the relative magnitude of these three components, defined as

$$\frac{\alpha_{xx}}{\alpha_{zz}} = r_1 \tag{15}$$

$$\frac{\alpha_{yy}}{\alpha_{zz}} = r_2. \tag{16}$$

The Raman scattering intensity ratios I_{aa}/I_{bb}, $I_{bb}/I_{c'c'}$, $I_{ab}/I_{c'c'}$, and $I_{bc}/I_{c'c'}$ are calculated from Equations 18–20 (Tsuboi et al. 1995a, 1995b; Ueda et al. 1996).

$$\frac{I_{aa}}{I_{bb}} = \frac{\alpha_{aa}^2}{\alpha_{bb}^2} = \frac{(l_x^2 r_1 + l_y^2 r_2 + l_z^2)^2}{(m_x^2 r_1 + m_y^2 r_2 + m_z^2)^2} \tag{17}$$

$$\frac{I_{bb}}{I_{c'c'}} = \frac{\alpha_{bb}^2}{\alpha_{c'c'}^2} = \frac{(m_x^2 r_1 + m_y^2 r_2 + m_z^2)^2}{(n_x^2 r_1 + n_y^2 r_2 + n_z^2)^2} \tag{18}$$

$$\frac{I_{ab}}{I_{c'c'}} = \frac{\alpha_{ab}^2}{\alpha_{cc}^2} = \frac{(l_x m_x r_1 + l_y m_y r_2 + l_z m_z)^2}{(n_x^2 r_1 + n_y^2 r_2 + n_z^2)^2}. \tag{19}$$

For a complete determination of the r_1 and r_2 values, normalized intensity ratios for I_{aa}/I_{bb}, $I_{bb}/I_{c'c'}$, and $I_{ab}/I_{c'c'}$ must be determined. For soluble species, the Raman depolarization ratio (ρ) provides additional constraints to determine r_1 and r_2. In this study, however, normalized intensity ratios from the edge faces (100) and (010) of dickite were not obtained because of the poor quality and small size of the crystals. The only normalized intensity ratios were obtained for I_{aa}/I_{bb} along the c' axis. Furthermore, the Raman depolarization ratio (ρ) is not defined for crystalline solids.

To simplify this problem for dickite, we assume that the out-of-plane polarizability components, α_{xx} and α_{yy}, are equal. This is equivalent to setting $r_1 = r_2$, which is replaced by the symbol r. Justification for this approximation is based on the nature of the OH oscillator. Because the primary atomic displacement is along the z axis, the greatest change in polarizability is expected to be along the z axis. In other words, the polarizability along the OH bond (z axis) is expected to be larger than the out-of-plane components along x and y.

$$\alpha_{zz} > \alpha_{xx} \approx \alpha_{yy} \tag{20}$$

and

$$r_1 = r_2 = r \tag{21}$$

Using Equations 18 and 22, we can simplify the expression for I_{aa}/I_{bb}

$$\frac{I_{aa}}{I_{bb}} = \frac{(l_x^2 r + l_y^2 r + l_z^2)^2}{(m_x^2 r + m_y^2 r + m_z^2)^2}. \tag{22}$$

The Eulerian angles and the direction cosine transformation matrices for the OH1 and OH3 groups are listed in Appendix Table 1. Using these values with the experimentally determined I_{aa}/I_{bb} ratio, the value of r can be solved for the OH1 and OH3 groups. The value of r for OH1 is 0.25 and that of the OH3 group is 0.47.